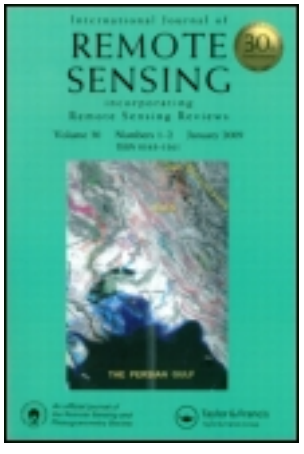

International Journal of Remote Sensing

Publication details, including instructions for authors and subscription information:
http://www.tandfonline.com/loi/tres20

Comparison and improvement of methods for identifying waterbodies in remotely sensed imagery

Fangdi Sun [a], Wanxiao Sun [b c], Jin Chen [d] & Peng Gong [e]

[a] International Institute for Earth System Science, Nanjing University, Nanjing, 210093, PR China

[b] Department of Geography and Planning, Grand Valley State University, Allendale, MI, 49401, USA

[c] State Key Laboratory of Remote Sensing Science, Institute of Remote Sensing Applications, Chinese Academy of Sciences, Beijing, 100101, PR China

[d] State Key Laboratory of Earth Surface Processes and Resource Ecology, Beijing Normal University, Beijing, 100875, PR China

[e] Centre for Earth System Science, Institute for Global Change Studies, Tsinghua University, Beijing, 100084, PR China

Available online: 14 Jun 2012

To cite this article: Fangdi Sun, Wanxiao Sun, Jin Chen & Peng Gong (2012): Comparison and improvement of methods for identifying waterbodies in remotely sensed imagery, International Journal of Remote Sensing, 33:21, 6854-6875

To link to this article: http://dx.doi.org/10.1080/01431161.2012.692829

International Journal of Remote Sensing
Vol. 33, No. 21, 10 November 2012, 6854–6875

Comparison and improvement of methods for identifying waterbodies in remotely sensed imagery

FANGDI SUN†, WANXIAO SUN*‡§, JIN CHEN¶ and PENG GONG|

†International Institute for Earth System Science, Nanjing University, Nanjing 210093, PR China

‡Department of Geography and Planning, Grand Valley State University, Allendale, MI 49401, USA

§State Key Laboratory of Remote Sensing Science, Institute of Remote Sensing Applications, Chinese Academy of Sciences, Beijing 100101, PR China

¶State Key Laboratory of Earth Surface Processes and Resource Ecology, Beijing Normal University, Beijing 100875, PR China

|Centre for Earth System Science, Institute for Global Change Studies, Tsinghua University, Beijing 100084, PR China

(*Received 24 May 2011; in final form 28 February 2012*)

This article first examines three existing methods of delineating open water features, i.e. the normalized difference water index (NDWI), the modified normalized difference water index (MNDWI) and a method combining the near-infrared (NIR) band and the maximum likelihood classification. We then propose two new methods for the fast extraction of water features in remotely sensed imagery. Our first method is a pixel-based procedure that utilizes indices and band values. Based on their characteristic spectral reflectance curves, waterbodies are grouped into three types – clear, green and turbid. We found that the MNDWI is best suited for identifying clear water. Green water has its maximum reflectance in Landsat Thematic Mapper (TM) band 4 (NIR band), whereas turbid water has its maximum reflectance in TM band 5 (mid-infrared band). Our second method integrates our pixel-based classification with object-based image segmentation. Two Landsat scenes in Shaanxi Province, China, were used as the primary data source. Digital elevation models (DEMs) and their derived slope maps were used as ancillary information. To evaluate the performance of the proposed methods, extraction results of the three existing methods and our two new methods were compared and assessed. A manual interpretation was made and used as reference data. Results suggest that our methods, which consider the diversity of waterbodies, achieved better accuracy. Our pixel-based method achieved a producer's accuracy of 92%, user's accuracy of 90% and kappa statistics of 0.91. Our integrated method produced a higher producer's accuracy (95%), but a lower user's accuracy (72%) and kappa statistics (0.72), compared with the pixel-based method. The advantages and limitations of the proposed methods are discussed.

*Corresponding author. Email: sunwa@gvsu.edu

International Journal of Remote Sensing
ISSN 0143-1161 print/ISSN 1366-5901 online © 2012 Taylor & Francis
http://www.tandfonline.com
http://dx.doi.org/10.1080/01431161.2012.692829

1. Introduction

Reliable information about the spatial distribution of open surface water is critically important in many scientific disciplines. For example, water information plays a vital role in the assessment of present and future water resources, climate models and agriculture suitability (Roberts *et al.* 1993, Voeroesmarty *et al.* 1997, Bastiaanssen *et al.* 2000). Some researchers also monitored waterbodies over large geographic areas on a periodic basis for land management and health agencies (Birketta and Mason 1995, Tran *et al.* 2010). Lehner and Doell (2004) created a global lakes and wetlands database that drew upon a variety of existing maps, data and information. The database is a combination of the best available sources for lakes and wetlands on a global scale (1:1 million to 1:3 million resolution). Ma *et al.* (2011) constructed a data set of China's lakes using 11 004 satellite images from the China–Brazil Earth Resources Satellite (CBERS) charge-coupled device (CCD) camera and Landsat Thematic Mapper (TM)/Enhanced Thematic Mapper (ETM+). However, the validation of these data sets requires an enormous amount of field survey and/or use of aerial photographs. Such approaches are both time- and labour-consuming.

Automated pixel-based methodologies have been used extensively to identify water features in moderate-resolution satellite imagery since the launch of Landsat-1 in 1972. Several studies used a single-band method (Work and Gilmer 1976, Rundquist *et al.* 1987). The single-band method involves selecting a band from a multispectral image. The near-infrared (NIR) band is usually chosen because NIR is strongly absorbed by water and is reflected strongly by terrestrial vegetation and dry soil. A threshold value is then determined subjectively for the band to distinguish between water and land. However, this method may lead to an overestimation or underestimation of open water area and the extracted water information is often mixed with shadows (McFeeters 1996).

Band-ratio methods use two bands from a multispectral image and take advantage of the differences in the spectral response of different land-cover types. In a simple ratio method, one band is taken from the visible bands such as the green band and is divided by the NIR band (Boland 1976). As a result, water features in the image are enhanced, whereas non-water features are suppressed. McFeeters (1996) developed the normalized difference water index (NDWI) method. The NDWI was derived using principles similar to those that were used to derive the normalized difference vegetation index (NDVI) (Townshend and Justice 1986). The NDWI is calculated as follows: NDWI = (Green – NIR) / (Green + NIR), where Green is a green band such as Landsat TM band 2 and NIR is an NIR band such as Landsat TM band 4. The NDWI index is designed to (1) maximize the reflectance of water features in the green band, (2) minimize the low reflectance of water features in the NIR band and (3) take advantage of the high reflectance of terrestrial vegetation and soil features in the NIR band. NDWI ranges from −1 to 1. Water features have positive values, whereas soil and terrestrial vegetation features have zero or negative values (McFeeters 1996). A main limitation of the NDWI method is that although the method can eliminate soil and terrestrial vegetation features in the image, it cannot efficiently suppress the signal from built-up land. As a result, extracted water features are often mixed with built-up land noise (Xu 2006).

Xu (2006) proposed a modified NDWI (MNDWI) in which a mid-infrared (MIR) band was used instead of the NIR band. The MNDWI can be expressed as follows: MNDWI = (Green – MIR)/(Green + MIR), where Green is a green band such as

Landsat TM band 2 and MIR is an MIR band such as Landsat TM band 5. MNDWI ranges from −1 to 1. Compared to the NDWI, water features have greater positive MNDWI values as they absorb more MIR light than NIR light. Soil, vegetation features and built-up land have negative values as they reflect more MIR light than green light (Jensen 2005, Xu 2006). Xu (2006) applied a threshold value of zero to extract water features from both NDWI and MNDWI images. He reported that the MNDWI was more suitable for the enhancement of water features with large amounts of built-up land in the background than the NDWI because it can efficiently reduce and even remove built-up land noise as well as terrestrial vegetation and soil features. Using multitemporal Landsat images, Hui *et al.* (2008) and Michishita *et al.* (2012) also used the NDWI and MNDWI to delineate waterbodies in a study of Poyang Lake, China.

Statistical pattern recognition techniques such as unsupervised and supervised classification methods have been widely used to extract land-use/land-cover features, including waterbodies (Sun *et al.* 2003, Sun 2004, Jensen 2005, Sirikulchayanon *et al.* 2008). Sivanpillai and Miller (2010) used the unsupervised Iterative Self-Organizing Data Analysis Technique (ISODATA) to detect waterbodies with Landsat and Advanced Spaceborne Thermal Emission and Reflection Radiometer (ASTER) imagery. They categorized waterbodies in the Powder River Basin of the USA into three types – clear, green and turbid. Green water refers to waterbodies in green colour. The green colour is due to the presence of submerged or floating vegetation. Turbid water may contain a lot of mud and appears to be brown (Sivanpillai and Miller 2010). Turbid water may result from a high concentration of suspended sediments or it may be a river that is shallow. The ISODATA approach is an automated process of grouping multi-band spectral response patterns into spectrally pure clusters. However, after the automated process the analyst must assign actual land-cover features (e.g. water) to the clusters by using field-collected and other available reference data, and experts are often required to identify and verify the results.

Multispectral classification based on the maximum likelihood algorithm is one of the most commonly used methods in the classification of remote-sensing imagery (McIver and Friedl 2002). Sheng *et al.* (2008) proposed a method to delineate water features that combines the NIR and the maximum likelihood classification (MLC). This method is called the NIR+MLC method in the rest of the article. The NIR band is used in the NIR+MLC method as water strongly absorbs NIR radiation and has a lower NIR reflectance compared to terrestrial features (Donald *et al.* 1987). Sheng *et al.* (2008) first applied a low threshold value to the NIR band of Landsat imagery to segment waterbodies from the background. They then refined the initial segmentation with MLC using all the available spectral information related to waterbodies. The MLC method has two major shortcomings. First, it only makes use of spectral information of terrain features while ignoring spatial information in the imagery. Second, the accuracy of multispectral classification depends to a large extent on the statistical assumption of normally distributed data, which is most often not met by the data used in image classification.

In addition to spectral features, geometric features (e.g. shape, size), texture and topographic features can also be used to enhance water information. Li (1995) introduced a shape index method to discriminate among various open water features, such as lakes, rivers and reservoirs. According to Niu *et al.* (2009), who compiled the wetland map of China including all of the waterbodies, 97.5% of the wetlands were located in areas with a slope less than 5° and 99.2% less than 8°. This suggests that slope is a key factor in the identification of waterbodies. Object-based classification has been

proposed as a means of incorporating such spatial information into the classification procedure (Wang *et al.* 2004).

Object-based image analysis (OBIA) or geospatial OBIA (GEOBIA), which emulates human interpreters' abilities, has been considered an automatic interpretation method since the late 1990s (Schiewe *et al.* 2001, Blaschke 2003). The application of the OBIA has increased sharply over the last several years as greater emphasis has been placed on deriving image objects with increasing spatial resolutions (Blaschke *et al.* 2008, Blaschke 2010). Classification units change from a single pixel in per-pixel analysis to image objects or objects that are made up of several pixels in OBIA. GEOBIA assumes that image objects provide a more appropriate scale to map environmental features. Note that objects can not only be derived from image data but also be developed from any spatially distributed variable, such as elevation and slope (Jensen 2005).

The GEOBIA approach involves two main steps: segmentation and classification (Wang *et al.* 2004). Image segmentation incorporates both spatial and spectral information to group similar image pixels into image objects or geo-objects with shape and spectral homogeneity (Benz 2001). Baatz and Schape (2000) developed one of the most promising approaches to remote-sensing image segmentation (Blaschke and Strobl 2001). Image objects can then be classified and related to real landscape features using object-based classification techniques (Blaschke *et al.* 2000, Hay *et al.* 2001, Yu *et al.* 2006). Frohn *et al.* (2005) used shape measures of compactness and smoothness in the segmentation process to distinguish thaw lakes from other water objects such as rivers and streams. Van der Werff and van der Meer (2008) took into account the shape measures of image objects such as compactness, roundness and convexity to classify rivers, lakes and reservoirs in Landsat imagery.

It is important to note that accuracy assessment strategies of the OBIA approach are different from the traditional pixel-based image analysis. Albrecht and his associates (Albrecht 2010, Albrecht *et al.* 2010) investigated the deviation of object boundaries between an OBIA land-use/land-cover classification and a reference data set using an object comparison approach, i.e. Object Fate Analysis (OFA) (Schoepfer *et al.* 2008, Tiede *et al.* 2010). Moreover, Grenier *et al.* (2008) proposed a method for calculating sampling size based on objects by considering the inherent variability within each wetland class.

A major advantage of GEOBIA is its capability to define criteria for image objects at set scales using spectral features, as well as texture, shape, context relationships and ancillary data of image objects at different spatial resolutions (Bock *et al.* 2005). Although the full advantage of the OBIA approach can be deployed with high-resolution image data, OBIA methods have also been utilized for medium- or coarse-resolution imagery, e.g. Landsat images (Dorren *et al.* 2003, Geneletti and Gorte 2003, Duveiller *et al.* 2008).

The objectives of this study are to (1) examine three existing methods of delineating open surface water, i.e. NDWI, MNDWI and NIR+MLC, (2) propose two new methods to extract water features from Landsat imagery and (3) compare and evaluate the performance of the existing methods and the proposed methods. Our first method is a pixel-based procedure that utilizes a series of indices and band values and is called the pixel-based method in the rest of the article. Our second method integrates the pixel-based classification and object-based image segmentation, which we call the integrated method. In this study, we adopted the three water types (clear, green and turbid) used

in Sivanpillai and Miller (2010). Green water may contain submerged or floating vegetation. Turbid water may contain a lot of mud or it may be heavily polluted. It should be noted that the primary purpose of our methods is to identify water-covered pixels rather than to differentiate different water types.

2. Study area and data preparation

2.1 *Study area*

The study area covers a part of Shaanxi Province in northwestern China (figure 1). The bounding latitudes of the study area are 33° 37′ N and 35° 35′ N and its bounding longitudes are 107° 35′ E and 111° 30′ E. This research is a pilot study of a global land-cover mapping project currently conducted in China. The global land-cover mapping project is called the 'High Resolution Global Land Cover Mapping Project for Global Environmental Change Studies and Earth Systems Simulation'. Shaanxi Province was selected as an experiment site due to its complex ecological characteristics. Shaanxi Province straddles across five ecological zones: Ordos Plateau steppe, Central China Loess plateau mixed forests, Huang He Plain mixed forests, Qin Ling Mountains deciduous forests and Daba Mountains evergreen forests (Kuang 2011). Landsat TM images were chosen as the experiment data.

Several mountains including Lishan, Huashan and Taibaishan run along the northern and southern edges of the study area, resulting in higher elevations in the north and the south and lower elevations in the middle. Taibaishan is the highest mountain in the study area, with its peak reaching about 3745 m. The average elevation of the central part is about 600 m. These mountains are partly covered with deciduous trees and coniferous forests. The mineral resources near the mountains are mainly coal, molybdenum and gold. A few opencast coalfields are scattered around, and the coal is exposed in the study area.

The study area features a temperate, semi-arid climate. The precipitation period of Shaanxi Province is between June and August. The rainfall during this period accounts for more than 40% of its annual precipitation. The influence of the terrains on precipitation is noticeable. The average annual precipitation is about 400–600 mm in the north, whereas it is about 500–700 mm in the south. Numerous natural and human-made waterbodies are found in the study area, including part of the Yellow River and its tributaries. The Yellow River is the second longest river in China. The river and many of its tributaries are very muddy and have a heavy sediment load. It has been estimated that nearly 90% of the sediment of the Yellow River comes from the Loess Plateau, composed of fine-grained silt (Ren and Shi 1986). The soil of the region has been called the 'most highly erodible soil on earth' (Laflen 2000). The sizes of the waterbodies in the study area vary from a single pixel to hundreds of thousands of pixels in a Landsat TM image. Other land-cover features include grassland, bare soil, pasture, farmland and urban areas.

2.2 *Data preparation*

Landsat images covering the entire Shaanxi Province were downloaded from the US Geological Survey (USGS) website (http://www.usgs.gov). Two Landsat 5 TM scenes were selected for this study and the path/row numbers are 126/36 and 127/36, respectively. Each of the two selected images has its unique features in terms of waterbodies. In the 126/36 scene, most of the waterbodies are in the natural environment because

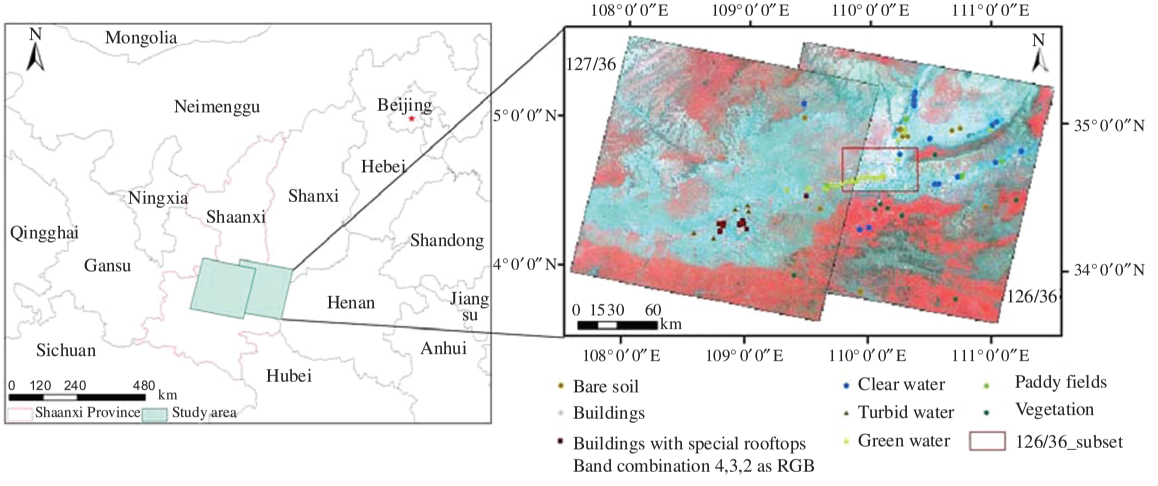

Figure 1. Location of the study area in Shaanxi Province, China: (*a*) the location of the study area in Shaanxi Province, China and (*b*) the two Landsat scenes used in the study.
Note: The symbols in this figure (circle, square, diamond and triangle) indicate the locations of selected sample features used to create figures 3, 4 and 5. 126/36 subset is chosen to display the classification results from different methods in figure 6.

this is mainly a mountainous area. On the other hand, the 127/36 scene contains several large and small urbanized areas such as Xian, Tongchuan, Weinan, Sanmenxia and Yuncheng. Therefore, waterbodies in the 127/36 scene have been influenced by varying degrees of anthropogenic activities. Anthropogenic activities often result in increasing eutrophication and the explosive growth of nuisance algae (Anderson and Garrison 1997). The urbanized areas have relatively low elevations. For example, the large metropolitan area of Xian is situated at about 400 m. Furthermore, waterbodies in the 127/36 scene appear to have a heavy sediment load carried down from the Loess Plateau. Phosphate fertilizer and nitrogen phosphorus compound fertilizer have been widely used for agriculture in the region, resulting in heavy pollution of waterbodies. Due to the weathering of bedrocks and soil erosion, some of the waterbodies in this region also contain considerable amounts of sands and soils.

The distinct features of the waterbodies in the two selected scenes provided a good basis for testing the robustness of the methods presented in this article. The 126/36 scene was acquired on 2 June 2007 and the 127/36 scene was acquired on 29 June 2009. These two images were selected because they contain minimal cloud cover and sensor noise. Another advantage of using images acquired in June is that during this month rivers and lakes in the study area are filled with more water and, therefore, there are more continuous water features in the imagery. This helps reduce the amount of mixed pixels around water features compared with the images acquired in drier months.

Six TM spectral bands, i.e. bands 1, 2, 3, 4, 5 and 7, were used in this research. TM band 6 was excluded due to its coarse spatial resolution. The images are in the Universal Transverse Mercator (UTM) Zone 49 N, World Geodetic System of 1984 (WGS 84). Digital elevation models (DEMs) from the Shuttle Radar Topography Mission (SRTM) corresponding to the two Landsat scenes were also used. The DEM data were downloaded from the SRTM 90 m Database (http://srtm.csi.cgiar.org). The 90 m spatial resolution DEM data were resampled to 30 m using a bilinear method to match the spatial resolution of Landsat images. To check the suitability of the SRTM data, we calculated statistics for the data and found that there was no exceptional value. The minimum value is 255 m and the maximum value is 3745 m. The SRTM elevation values represent the topography of the study area well. Using the state 1:50 000 DEM and 1:250 000 DEM as references, Zhan (2008) evaluated the SRTM data of Shaanxi Province and reported that the accuracy of surface parameters such as slope and aspect based on SRTM DEM is always higher than that based on the 1:250 000 DEM but lower than that based on the 1:50 000 DEM. The maximum error of the derived slope values from the SRTM DEM is larger (about 8°) in steep mountain regions than in flat areas (about 3°) in the entire Shaanxi Province. Waterbodies are generally located in flat regions which have low slope values. Therefore, it is reasonable to use the SRTM data to refine our result.

Atmospheric and topographic correction of the selected images was carried out using Atmospheric and Topographic Correction (ATCOR) software. ATCOR is an add-on module to ERDAS IMAGINE that eliminates atmospheric and illumination effects in imagery (ERDAS Inc. 2010). Atmospheric correction involves two major steps: parameter estimation and surface reflectance retrieval (Liang *et al.* 2001). ATCOR is a large database containing the results of radiative transfer calculations based on the Moderate Resolution Atmospheric Transmission (MODTRAN) code (Berk *et al.* 1998, 2003). MODTRAN is a radiative transfer program designed to model atmospheric propagation of electromagnetic radiation for the 0.2–100 μm spectral range. ATCOR performs atmospheric correction for image data by inverting

results of MODTRAN calculations compiled in a database. The look-up tables in the database consist of the following parameters: standard atmospheres (altitude profile of pressure, air temperature, water vapour content, ozone concentration), aerosol types, a range of aerosol concentrations, a range of ground elevations and solar zenith angles (ERDAS Inc. 2011).

3. Methods

3.1 *Existing methods*

To evaluate the performance of different approaches, we first adopted three existing methods, i.e. the NDWI (McFeeters 1996), MNDWI (Xu 2006) and NIR+MLC (Sheng *et al.* 2008), to extract water features from the two Landsat images. The NDWI was implemented by using TM band 2 (green) and TM band 4 (NIR). TM band 2 (green) and TM band 5 (MIR) were used in the implementation of the MNDWI method. A threshold value of zero was applied to the NDWI and MNDWI images to separate water features from the background.

The NIR+MLC method proposed by Sheng *et al.* (2008) was implemented in two steps. First, a low threshold value of 0.25 was applied to the NIR band to separate waterbodies from the background. Pixels having values lower than the threshold are considered water pixels; those whose values are greater than or equal to the threshold are considered background pixels. To avoid underestimation of surface water in the final results, we relaxed the threshold and increased its value to 0.5. As a result, some other land-cover types with low NIR values were also classified as water pixels. The subsequent MLC aimed to distinguish between water and other land-cover types.

Second, MLC was applied to all the spectral bands, and a map of open surface water was obtained for each of the Landsat scenes. As we are only interested in water features, two classes are necessary, i.e. water and non-water/others. Training samples of about 500 water pixels and 1000 non-water pixels were selected in each Landsat scene. A larger number of non-water pixels were used because the area of non-water features is larger than that of the waterbodies in both scenes. Furthermore, a team of China's global land-cover mapping project, mentioned above, carried out field work in the study area in June 2010. One of the main purposes of the field work was to collect training samples for different land-cover types. Our field work shows that clear, green and turbid waterbodies are all present in the 127/36 scene, whereas the 126/36 scene mainly contains clear and green water features. It should be noted that the selected training samples were not differentiated between clear, green and turbid water. In other words, all the three water types were lumped together as water. A detailed description of clear, green and turbid water is provided in the following section. Experience and knowledge of the study area were utilized in the selection of training samples. For example, particular attention was paid to the selection of certain non-water features such as shadows and coalfields as they tend to have similar spectral reflectance to water.

3.2 *New pixel-based method*

This method is a pixel-based procedure that utilizes indices and band values. In view of the diversity of waterbodies in the study area, we grouped water into three types – clear, green and turbid. We found that these three types of water have distinctive spectral reflectance characteristics. The reflectance of clear water decreases as the wavelength

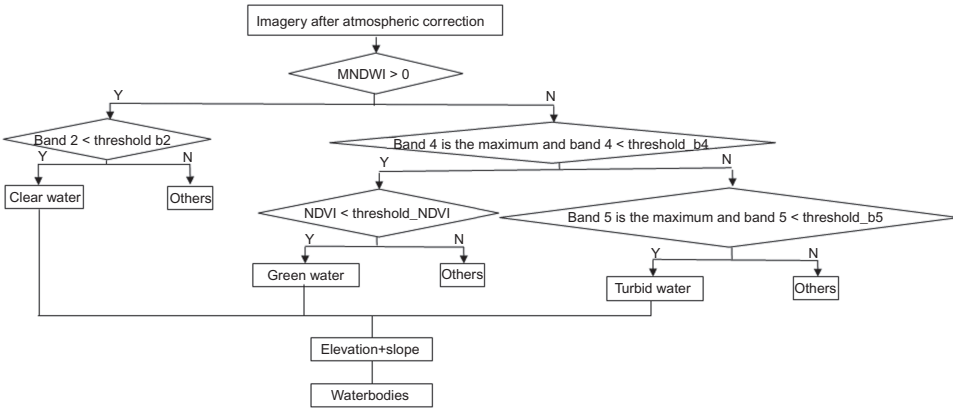

Figure 2. Flow chart of the new pixel-based method for extracting clear, green and turbid waterbodies.
Note: Threshold_b2 represents a threshold value in TM band 2, threshold_b4 represents a threshold value in TM band 4, threshold_b5 represents a threshold value in TM band 5 and threshold_NDVI represents a threshold value of NDVI.

increases. Green water has its maximum reflectance in TM band 4, whereas turbid water has its maximum reflectance in TM band 5. Therefore, these three types of water can be identified based on their unique spectral reflectance curves. The main steps in the proposed method are displayed in figure 2. As figure 2 illustrates, there are three approaches in the flowchart for identifying the three water types. After these water types have been identified, elevation and slope data are used to exclude certain non-water features such as easily confused coalfields and shadows. Details about the extraction of each water type are discussed in the following sections.

3.2.1 Extraction of clear water. A significant characteristic of clear water is that its spectral reflectance decreases as the wavelength increases. This means that, for clear water features, the difference between the values of TM bands 2 and 5 is greater than the difference between the values of TM bands 2 and 4 (figure 3). In other

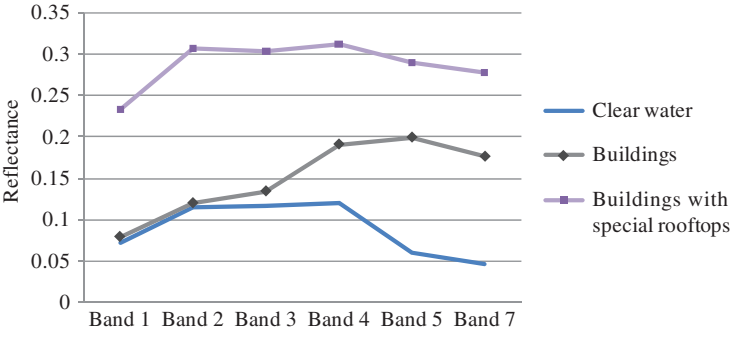

Figure 3. Average spectral reflectance patterns of clear water, regular buildings and buildings with special rooftops.

words, clear water features have greater positive MNDWI values than their NDWI values. Therefore, the MNDWI was chosen to extract clear water features in the two Landsat images. A threshold value of zero was used to separate clear water from the background.

Another reason why the MNDWI was chosen is that this method is more effective in eliminating built-up land noise (Xu 2006). As can be seen in figure 3, it is fairly easy to distinguish clear water from regular buildings as these buildings have negative MNDWI values. However, we observed that some confusion occurred between clear water and those buildings with special rooftops that are made of metals or are painted in particular colours. This confusion was caused by the fact that the buildings with special rooftops also have positive MNDWI values. We further observed that the spectral reflectance of clear water is usually lower in band 2 (about 7.5% lower) than that of the buildings with special rooftops. Therefore, in addition to the MNDWI, we applied a low threshold to TM band 2 (green band) to exclude those buildings. It should be noted that each spectral reflectance curve in figure 3, clear water, for example, represents the average spectral reflectance of its corresponding land-cover feature. The locations of the sample sites representing each land-cover type are marked in figure 1. Similarly, figures 4 and 5 discussed in the following two sections depict the

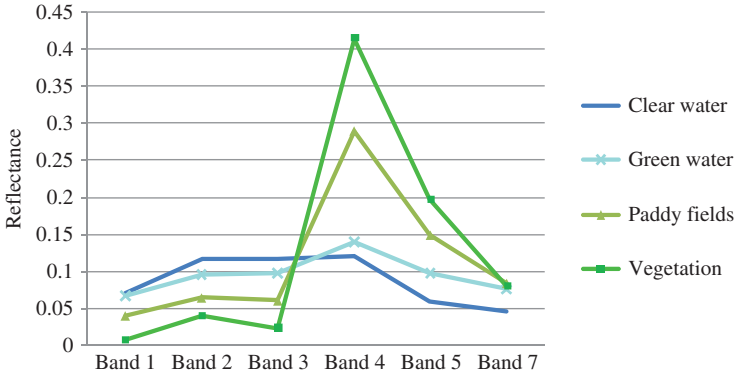

Figure 4. Average spectral reflectance patterns of clear water, green water, terrestrial vegetation and paddy fields.

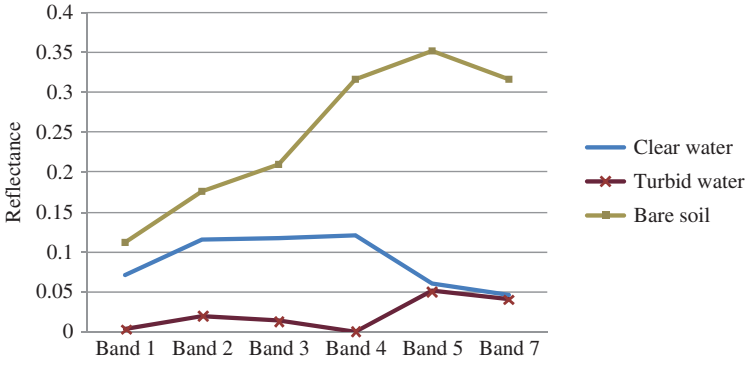

Figure 5. Average spectral reflectance patterns of clear water, turbid water and bare soil.

mean spectral reflectance of their corresponding land-cover features. Sample locations for these land-cover types are also shown in figure 1.

3.2.2 Extraction of green water. Green water differs from clear water and turbid water in that its maximum spectral reflectance value occurs in the NIR band (TM band 4). Therefore, TM band 4 is chosen to distinguish green water from other water features. A major challenge to the identification of green water is the similarity between green water and terrestrial vegetation in terms of their spectral reflectance characteristics. Both green water and terrestrial vegetation absorb much light in the red band (TM band 3) and reflect strongly in the NIR band (TM band 4) due to the presence of chlorophyll (figure 4). A noteworthy difference between green water and terrestrial vegetation is that green water has a much lower reflectance value in the NIR band. Therefore, we used the following two conditions to extract green water pixels: (1) their maximum values occur in TM band 4 and (2) their pixel values in TM band 4 are smaller than a certain threshold.

Another problem we encountered was that the paddy fields in the study area also have low reflectance in the NIR band (figure 4). To overcome this problem, the NDVI was further used to separate green water from paddy fields. Paddy fields have higher NDVI values than green water. The NDVI is calculated as follows: $\mathrm{NDVI} = (\mathrm{NIR} - \mathrm{RED})/(\mathrm{NIR} + \mathrm{RED})$, where NIR is TM band 4 and RED is TM band 3.

3.2.3 Extraction of turbid water. Turbid water differs from clear water and green water in that its maximum spectral reflectance value occurs in TM band 5 (MIR band). However, bare soil also has its highest spectral reflectance in TM band 5 (figure 5). Nevertheless, the spectral reflectance of turbid water in TM band 5 is much lower than that of bare soil. Therefore, turbid water can be identified using the following conditions: (1) pixels whose highest reflectance is in TM band 5 and (2) pixels whose reflectance values in TM band 5 are lower than a certain threshold.

3.2.4 Use of DEM data. Using the above three steps, open surface water including clear, green and turbid was extracted. However, shadows in mountainous areas were often mixed with water features due to their similar spectral responses. A good strategy for dealing with this problem is to incorporate ancillary DEM data. We first generated a slope image from the DEM data for each of the two Landsat scenes. Based on the knowledge that waterbodies are located in areas with low elevations and small slopes, we then set-up elevation and slope thresholds to remove shadows in mountainous areas.

Pixel-based classification makes use of the spectral response of every single pixel in the image. This approach often results in 'salt-and-pepper' effects and weakly defined inter-region boundaries on the classified map (Solaiman *et al.* 1998, Sun *et al.* 2003). For instance, the inner portion of the extracted lakes may contain non-water pixels. To reduce such 'salt-and-pepper' noise, we experimented with several threshold values. However, this approach may lead to an overestimation or underestimation of water information. As such, we proposed a second method that incorporates image segmentation procedure to improve classification results.

3.3 *Integration of pixel-based method and object-based segmentation*

Our second method begins with the segmentation of the two Landsat images using an object-based segmentation procedure. The segmentation was performed using eCognition software from Trimble (http://www.ecognition.com). Specifically, the multiresolution segmentation algorithm was used. It is a bottom-up segmentation algorithm in which pixels or image objects are merged consecutively based on a pairwise region merging technique (Definiens 2009). This algorithm locally minimizes the average heterogeneity of image objects for a given resolution of image objects and maximizes their respective homogeneity (Definiens 2009).

The algorithm requires three user-defined parameters: (1) scale parameter, (2) shape factor and (3) compactness. Scale parameter is a threshold of heterogeneity that controls the degree of heterogeneity within an image object. A higher scale parameter leads to larger and less homogeneous objects, and vice versa. Heterogeneity is defined in terms of two factors: spectral (colour) values and shape. These two factors can be interactively weighted by the user: the higher the shape factor, the lower the influence of spectral values in the segmentation. The shape factor is further described by two landscape ecology metrics: compactness and smoothness. These two metrics can also be weighted by the user: the higher the compactness value, the lower the smoothness value. Platt and Rapoza (2008) reported that there is no effective method to select optimal parameters for image segmentation. In this study, we aimed to generate a small size of image objects so that small water features would not be lost during the integration process described below. We performed a lot of trial-and-error attempts with the three user-defined parameters until the resulting objects closely corresponded to the boundaries of landscape features.

The image objects obtained from the above segmentation process were then overlaid with the pixel-based classification results. An algorithm integrating the pixel-based classification and the object-based segmentation was developed. The algorithm performed the following operations within each image object that resulted from the image segmentation procedure.

1. Calculating the percentage of water pixels from the pixel-based classification results within each image object.
2. Defining a percentage threshold, such as 20%, 15% and 10%, which was then used to compare with the percentage of water pixels within each image object.
3. Making comparisons and assigning new values to the final output image using the following criteria: if the percentage of water pixels was greater than a certain threshold (e.g. 10%), then the image object was assigned to the 'water' class. Otherwise, the object was assigned to the 'non-water' or 'others' class.

4. Results and discussion

Using the five methods discussed above, the two Landsat scenes were classified into two classes: water and non-water. To evaluate the performance of these methods, pixel-by-pixel comparison was made between each automatic extraction result and a reference data set, which was derived from visual image interpretation. The two Landsat images were visually interpreted by one person and checked by another, and both were familiar with the study area. The interpretation was carried out according to the spectral, spatial and contextual information and the DEM data and its derived

Table 1. Accuracy assessment of waterbodies in the two entire Landsat scenes using the five methods, i.e. NDWI, MNDWI, NIR+MLC, new pixel-based method and new integrated method.

		NDWI	MNDWI	MLC+NIR	New pixel-based method	New integrated method
126/36	Producer's accuracy (%)	36.29	86.33	91.34	92.22	95.11
	User's accuracy (%)	98	95.31	89.28	90.61	72.01
	Overall accuracy (%)	99.55	99.87	99.86	99.88	99.71
	Overall kappa	0.5279	0.9054	0.9023	0.9135	0.8182
	Kappa (water)	0.9799	0.9527	0.8921	0.9054	0.7181
127/36	Producer's accuracy (%)	82.01	29.85	79.17	74.46	85.51
	User's accuracy (%)	57.51	68.54	73.99	83.52	60.2
	Overall accuracy (%)	99.80	99.79	99.88	99.90	99.82
	Overall kappa	0.6751	0.4150	0.7643	0.7868	0.7057
	Kappa (water)	0.5740	0.6846	0.7392	0.8348	0.6010

slope data. Google Earth was also used to assist in the visual interpretation of the images. Producer's accuracy, user's accuracy and kappa statistics were calculated for each of the five methods. As the area of the non-water class, which is considered the background, is much larger than the water, the overall accuracies of these methods are all greater than 99% and have only minor differences. Table 1 summarizes classification accuracy and kappa statistics for waterbodies in the two images using the five methods.

For the purpose of comparison, the three types of water (clear, green, turbid) extracted using the pixel-based method were combined into just one class, i.e. water. Figure 6(*a*) shows the result from visual image interpretation. Figures 6(*b*)–(*f*) display the classification results from the five methods for a subset of the Landsat 126/36 scene, which is marked in figure 1. The subset consists of 1876 × 1102 pixels and its bounding latitudes are 34° 19′ N and 34° 27′ N and bounding longitudes 108° 49′ E and 109° 3′ E.

4.1 *NDWI and MNDWI*

As can be seen from table 1, overall the NDWI worked better for the 127/36 scene, whereas the MNDWI worked better for the 126/36 scene. The difference in the performance of the NDWI and MNDWI can be attributed to the characteristics of land cover/land use in general and the waterbodies in particular in the two images. The 127/36 scene contains several cities and, therefore, is characterized by fragmented small patches of various urban land-cover types. As such, there are lots of mixed pixels in the scene due to the 30 m resolution of the Landsat imagery. Many of the mixed pixels in this scene contain a built-up land component.

Waterbodies in the 127/36 scene are relatively turbid as they are strongly affected by a high level of urbanization and/or sediment concentration. The NDWI can extract those water pixels whose TM band 2 (green) values are higher than their band 4 (NIR) values. Both clear and turbid water meet this criterion and, therefore, the NDWI extracted most turbid and clear water in the 127/36 scene. The NDWI achieved a

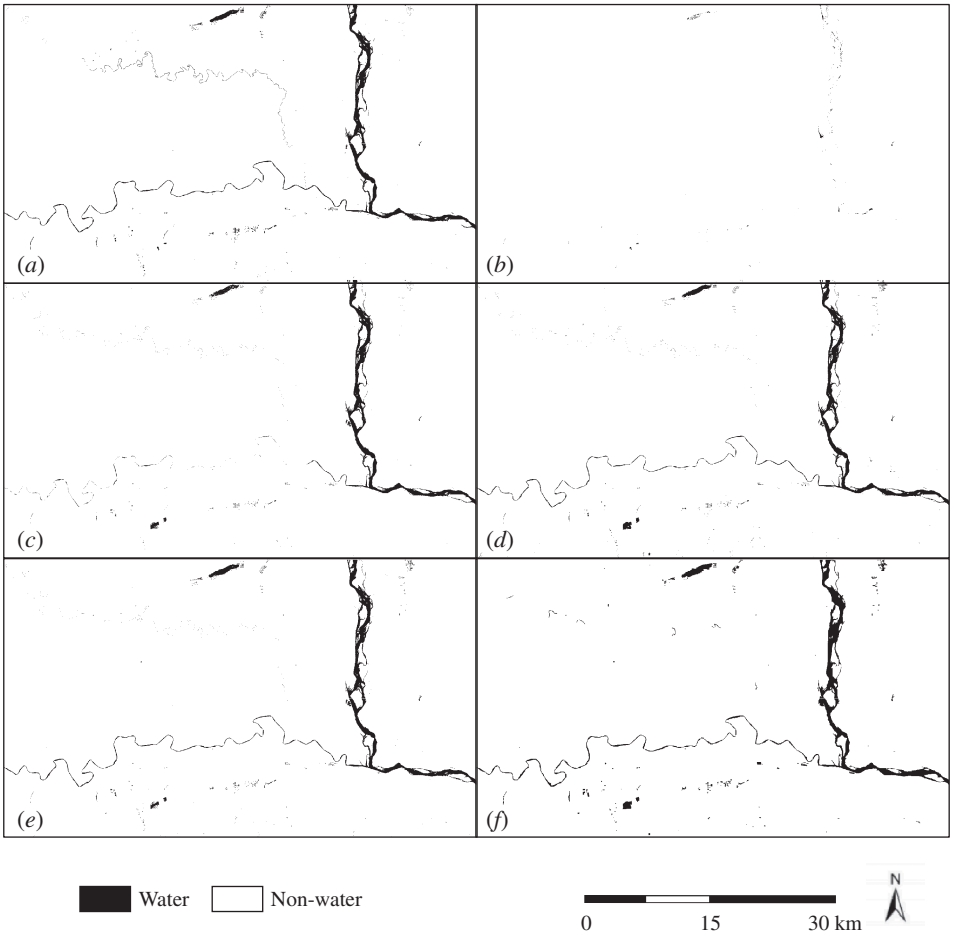

Figure 6. Results for a subset of the 126/36 scene using different methods: (*a*) visual image interpretation, (*b*) NDWI, (*c*) MNDWI, (*d*) NIR+MLC, (*e*) new pixel-based method and (*f*) new integrated method.

producer's accuracy of 82.0%, a user's accuracy of 57.5% and a kappa statistics of 0.57. The MNDWI can extract those water pixels whose TM band 2 (green) values are higher than TM band 5 (MIR) values. The MNDWI was able to identify a small number of clear waterbodies in this scene, but it could not extract most of the turbid water as the turbid water has its highest reflectance in band 5 (MIR) (figure 5). The MNDWI only achieved a user's accuracy of 68.5%, a low producer's accuracy of 29.8% and a kappa statistics of 0.68. Although the kappa statistics of water that resulted from the NDWI method is slightly higher than that from the MNDWI, overall kappa statistics of the NDWI is much higher than that of the MNDWI, i.e. 0.68 vs 0.42. We observed that along the edges of water features such as rivers, lakes and channels, many pixels contain both turbid water and built-up land. It is likely that the band 5 values of these mixed pixels are greater than their band 2 values due to the high band 5 value of the built-up land (figure 3). As a result, these mixed pixels of water and built-up land cannot be extracted using the MNDWI.

The 126/36 scene covers a mountainous region where elevations are higher and there is relatively less human activity. Because of high elevations of the mountains, sediment concentration in waterbodies is much lower compared with that at lower elevations. Vegetation often grows near or along the edges of water features in this scene. Therefore, the water features in this scene are mostly clear and green water. The MNDWI performed well for this scene, and the producer's accuracy, user's accuracy and kappa statistics were 86.3%, 95.3% and 0.95, respectively. The NDWI achieved a user's accuracy of 98%, but a lower producer's accuracy of 36.3% and a kappa statistics of 0.98. The overall kappa statistics from the MNDWI is much higher than that from the NDWI, i.e. 0.91 vs 0.53. We observed that the 126/36 scene contains many mixed pixels, and many of the mixed pixels contain both clear water and vegetation. As a result, the spectral reflectance of these mixed pixels is quite similar to green water. It is likely that band 4 values of these mixed pixels of clear water and vegetation are greater than their band 2 values. Thus, such water–vegetation mixed pixels cannot be extracted using the NDWI.

4.2 *NIR+MLC*

The NIR+MLC method achieved a better result for the 126/36 scene than for the 127/36 scene (table 1). The producer's accuracies for the 126/36 and 127/36 scenes are 91.3% and 79.2% respectively, representing about 11% difference. Overall kappa statistics and the kappa statistics of water are both higher for the 126/36 scene than for the 127/36 scene, i.e. 0.90 vs 0.76 and 0.89 vs 0.74. There are several factors that may explain this difference such as water type, size and depth. As discussed above, the 126/36 scene consists mainly of clear and green water and is rather homogeneous. The high elevation of this scene leads to less sediment concentration in the waterbodies. On the other hand, the 127/36 scene contains all types of water. Although this research classified water into three types (clear, green, turbid), it is quite possible that certain water features lie somewhere between these three types in terms of their colours. This means that our training samples may not have included all the water types present in the study area, resulting in a lower classification accuracy.

Compared to the 127/36 scene, more natural waterbodies are found in the 126/36 scene, and the size of waterbodies is generally larger. As such, more water-mixed pixels exist in the 127/36 scene, which degraded the classification accuracy of the scene. The term water-mixed pixels is used here to refer to pixels that spatially cover both water and non-water features. In fact, the total radiance of a waterbody recorded by a remote sensor is a function of water-surface radiance, subsurface volumetric radiance and radiance from the bottom of the waterbody (Bukata *et al.* 1995). Waterbodies in the 127/36 scene are rather shallow. Therefore, if the waterbody itself is not deep enough, the sensor can get spectral responses from the bottom of the waterbody. This may further explain the lower classification accuracy for the 127/36 scene compared to the 126/36 scene.

4.3 *New pixel-based method*

Our new pixel-based method requires selecting threshold values to separate water features from other land-cover types. The classification results from the pixel-based method are displayed in figure 6(*e*). These results are obtained using the following thresholds: (1) a TM band 2 value of less than 0.18 was used to extract clear water pixels, (2) a TM band 4 value of smaller than 0.2 and a NDVI value of less than 0.3

were used to identify green water, (3) a TM band 5 value of less than 0.15 was used to obtain turbid water and (4) slopes less than 20° and elevations lower than 1000 m were used to remove shadows in mountainous areas. These threshold values were chosen on the basis of experiments and visual comparisons of classification results.

Overall, the pixel-based method performed well for the two Landsat images. The method achieved a better result for the 126/36 scene than for the 127/36 scene (table 1). Compared with the three existing methods, our pixel-based method yielded a higher producer's accuracy for the 126/36 scene. Specifically, the producer's accuracy of the pixel-based method is 55% higher than that of the NDWI and about 5.9% higher than that of the MNDWI. The method also represents an improvement over the NIR+MLC. In fact, the pixel-based method is the only procedure whose producer's accuracy and user's accuracy are higher than 90% for the 126/36 scene. Furthermore, the overall kappa statistics and the kappa statistics of water of this method are greater than 0.90 for the 126/36 scene. This shows that the pixel-based method is better able to identify clear and green waterbodies than the other methods tested in this study.

For the 127/36 scene, the pixel-based method achieved the highest overall kappa statistics (0.79), water kappa statistics (0.83) and user's accuracy (83.5%) among all the five methods. For this scene, the producer's accuracy of the pixel-based method (74.4%) is about 44% higher than that of the MNDWI (29.8%). However, it is slightly lower than the NDWI and the MLC+NIR by about 7.5% and 4.7%, respectively. These results suggest that the pixel-based method does not perform as well as the NDWI and MLC+NIR when a large number of turbid water pixels and water and built-up land-mixed pixels exist in the image.

4.4 *Integration of pixel-based method and object-based segmentation*

Figure 6(*f*) shows the classification result from our integrated method. The segmentation was done using a scale parameter of 15, a shape factor of 0.1 and a compactness of 0.5. A percentage threshold of 10% was then applied in the algorithm to integrate the pixel-based classification and the image objects. A significant improvement achieved with the integrated method is that the 'salt-and-pepper' noise disappeared and areas of water features became more homogeneous. Compared to the pixel-based classification, the producer's accuracy of the integrated method increased by about 11% (from 74% to 85%) for the 127/36 scene and 3% (from 92% to 95%) for the 126/36 scene (table 1). Among the five methods, the integrated method achieved the highest producer's accuracy for both scenes, i.e. 95% for the 126/36 scene and 85.8% for the 127/36 scene.

As can be seen from table 1, the user's accuracy, the overall kappa statistics and the kappa statistics of water of the integrated method were lower than those of the pixel-based method for both scenes. The overestimation of water features in the integration process is mainly responsible for the lower accuracy of the integrated method. As discussed above, a considerable number of pixels in the 127/36 scene contain both water and built-up land, and many pixels in the 126/36 scene contain both water and vegetation. Some of these mixed pixels, especially those along the edges of water features such as rivers and lakes, have been reclassified as water pixels in the process of integrating the results from image segmentation and the pixel-based method. For instance, if a water–vegetation mixed pixel is part of an image object that was identified as water, then that mixed pixel would be reclassified as a water pixel. A closer examination of the

classification results further suggests that the integrated method misclassified certain features such as shadows and coalfields as waterbodies in the study area.

As discussed in the Introduction, Albrecht and his associates (Albrecht 2010, Albrecht *et al.* 2010) developed OBIA-specific accuracy assessment strategies. For example, spatial uncertainty in object delineation was measured by an epsilon error band with OFA (Zhang and Goodchild 2002). Different accuracy may be obtained if such a method was used.

5. Conclusions

Information and knowledge of the Earth's surface water is increasingly needed by both practitioners and scientists in water resource management and global change research. This study tested two proposed methods as well as three existing methods for the extraction of water features in remotely sensed data. Results from the NDWI and MNDWI methods suggest that the use of a single index cannot fully achieve the goal of accurately delineating open surface water. The NDWI and MNDWI complement each other and, therefore, should be used to extract different types of water features.

Compared with the NDWI and MNDWI, the MLC+NIR method achieved higher accuracies, but it was a time-consuming procedure. The method requires the analyst to have considerable experience in image processing and good knowledge of the study area. To achieve satisfactory classification results, it is often necessary to adjust the types and numbers of training samples. Therefore, the stability of this method is poor.

The two proposed new methods utilize more spectral information in the image than do the NDWI or MNDWI methods. The new methods are faster to implement than the NIR+MLC method as they do not require training samples. Overall, the proposed methods performed well for the two Landsat images used in this study. They demonstrated improvements of varying degrees over the existing methods. Despite these encouraging results, more work clearly is needed to further improve the robustness of the proposed methods. For example, the two proposed methods as well as the three existing methods require the choosing of certain threshold values to extract water features in the image. The thresholds used in this study were determined based on the analyst's experience and visual comparisons of classification results. It is clear that a more robust approach is needed to objectively determine optimum thresholds for the proposed methods in future research. The pixel-based method can be applied to other remote-sensing imagery such as Landsat images in a different region. This is because the pixel-based method is based on the physical principle of electromagnetic radiation of water features. Atmospheric correction must be performed before applying the method. The threshold values used in this study may be changed considering such factors as the variation of solar zenith angle and atmospheric condition in a particular region.

Another direction in which the present research can be expanded is to develop a more comprehensive system for categorizing water features in remotely sensed data. In this study, we classified the waterbodies in the study area into three (colour) types, i.e. clear, green and turbid. This research has revealed that the strategy of grouping waterbodies into different types is necessary and effective. Open surface water varies considerably in terms of its morphological and biochemical characteristics as well as size and location. Categorization of open surface water for image classification purposes is an issue that deserves further research.

Our results suggest that shadows, coalfields and dry valleys are often misclassified as waterbodies due to their similar spectral reflectance characteristics. In this study, we utilized ancillary DEM and slope information to remove the noise caused by shadows in mountainous areas. This strategy proves effective in improving classification results. It seems desirable that future research should include other ancillary information to deal with such sources of noise as coalfields and dry valleys.

This research has also revealed that water features are often mixed with other land-cover/land-use types such as built-up land and vegetation in remotely sensed images. The proposed methods cannot effectively deal with the mixed pixel problem. Advanced classification algorithms, such as linear spectral unmixing, fuzzy classification logic and the support vector machine, may be used in future research to improve classification accuracies. To obtain more accurate classification results, satellite images that have both high spatial and spectral resolution may also be needed.

It should be noted that the object-based segmentation process generates not only homogeneous image objects but also several attributes for each image object. These attributes include area, length, length width ratio, roundness, elliptic fit and compactness. Such shape measures as well as spectral, contextual and other information may be incorporated in an object-based procedure to improve classification accuracies. To what extent the use of such object-based classification techniques can more effectively extract water features is another issue that requires further research. Furthermore, the segmentation parameters we used may not be optimal. Dragut *et al.* (2010) presented a technique for estimating the scale parameter for multiresolution image segmentation of remotely sensed data with eCogniton. The tool, called Estimation of Scale Parameter (ESP), enables the selection of appropriate scales objectively for image segmentation (Dragut *et al.* 2010). Future research may also consider using such a technique.

Acknowledgements

This research was supported by the following grants: the National High Technology Research and Development Programme of China (No. 2009AA12Z1462 and No. 2008AA121702) and State Key Laboratory of Remote Sensing Science, Institute of Remote Sensing Applications, the Chinese Academy of Sciences (No. OFSLRSS201015). The authors thank the technology research group of the National High Technology Research and Development Programme of China for data collection and image preprocessing. They also thank Professor Arthur Cracknell, Co-Editor-in-Chief of the International Journal of Remote Sensing, and two anonymous reviewers for their very helpful suggestions and comments on an earlier draft of this article.

References

Albrecht, F., 2010, Uncertainty in image interpretation as reference for accuracy assessment in object-based image analysis. In *Proceedings of the Ninth International Symposium on Spatial Accuracy Assessment in Natural Resources and Environmental Sciences*, 20–23 July 2010, N.J. Tate and P.F. Fisher (Eds.), Leicester, UK (Bodmin: MPG Books Group), pp. 13–16.

Albrecht, F., Lang, S. and Hölbling, D., 2010, Spatial accuracy assessment of object boundaries for object-based image analysis. In *Third International Conference on All Aspects of Geographic Object-Based Image Analysis*, 29 June–2 July, Ghent, Belgium.

Anderson, D.M. and Garrison, D.J., 1997, The ecology and oceanography of harmful algal blooms. *Limnology and Oceanography*, **42**, pp. 1009–1305.

Baatz, M. and Schäpe, A., 2000, Multiresolution segmentation: an optimization approach for high quality multi-scale image segmentation. In *Angewandte Geographische Informationsverarbeitung XII*, J. Strobl, T. Blaschke and G. Griesebner (Eds.), pp. 12–23 (Heidelberg: Wichmann-Verlag).

Bastiaanssen, W.G.M., Molden, D.J. and Makin, I.W., 2000, Remote sensing for irrigated agriculture: examples from research of possible applications. *Agricultural Water Management*, **46**, pp. 137–155.

Benz, U., 2001, Definiens imaging gmbH: object-oriented classification and feature detection. *IEEE Geoscience and Remote Sensing Society Newsletter*, September, pp. 16–20.

Berk, A., Anderson, G.P., Acharya, P.K., Hoke, M.L., Chetwynd, J.H., Bernstein, L.S., Shettle, E.P., Matthew, M.W. and Adler-Gloden, S.M., 2003, *Modtran Version 3 Revision 1 User's Manual* (Hanscom, MA: Air Force Research Laboratory).

Berk, A., Bernstein, L.S., Anderson, G.P., Acharya, P.K., Robertson, D.C., Chetwynd, J.H. and Adler-Gloden, S.M., 1998, Modtran cloud and multiple scattering upgrades with application to AVIRIS. *Remote Sensing of Environment*, **65**, pp. 367–375.

Birketta, C.M. and Mason, I.M., 1995, A new global lakes database for a remote sensing program studying climatically sensitive large lakes. *Journal of Great Lakes Research*, **21**, pp. 307–318.

Blaschke, T., 2003, Object-based contextual image classification built on image segmentation. In *Proceedings of the 2003 IEEE Workshop on Advances in Techniques for Analysis of Remotely Sensed Data*, 27–28 October 2003, Washington, DC (Piscataway, NJ: IEEE), pp. 113–119.

Blaschke, T., 2010, Object based image analysis for remote sensing. *ISPRS Journal of Photogrammetry and Remote Sensing*, **65**, pp. 2–16.

Blaschke, T., Lang, S. and Hay, G.J., 2008, *Object-Based Image Analysis: Spatial Concepts for Knowledge Driven Remote Sensing Applications* (Heidelberg: Springer-verlag).

Blaschke, T., Lang, S., Lorup, E., Strobl, J. and Zeil, P., 2000, Object-oriented image processing in an integrated GIS/remote sensing environment and perspectives for environmental applications. In *Environmental Information for Planning, Politics and the Public*, A. Cremers and K. Greve (Eds.), pp. 555–570 (Marburg: Metropolis-verlag).

Blaschke, T. and Strobl, J., 2001, What's wrong with pixels? Some recent developments interfacing remote sensing and GIS. *GIS*, **6**, pp. 12–17.

Bock, M., Xofis, P., Mitchley, J., Rossner, G. and Wissen, M., 2005, Object-oriented methods for habitat mapping at multiple scales – case studies from Northern Germany and Wye Downs. *UK Journal for Nature Conservation*, **13**, pp. 75–89.

Boland, D.H.P. (Ed.), 1976, *Trophic Classification of Lakes Using Landsat-I (ERTS-l) Multispectral Scanner Data* (Corvallis, OR: United States Environmental Protection Agency, Office of Research and Development, Corvallis Environmental Research Laboratory).

Bukata, R.P., Jerome, J.H., Kondratyev, K.Y. and Pozdnyakov, D.V., 1995, *Optical Properties and Remote Sensing of Inland and Coastal Waters*, 362 p. (New York: CRC Press).

Definiens, 2009, *Definiens eCognition Developer 8 – User Guide* (Muenchen: Definiens AG).

Dorren, L.K., Maier, B. and Seijmonsbergen, A.C., 2003, Improved Landsat-based forest mapping in steep mountainous terrain using object-based classification. *Forest Ecology and Management*, **183**, pp. 31–46.

Dragut, L., Tiede, D. and Levick, S., 2010, A tool to estimate scale parameters for multiresolution image segmentation of remotely sensed data. *International Journal of Geographical Information Science*, **24**, pp. 859–871.

Duveiller, G., Defourny, P., Desclee, B. and Mayaux, P., 2008, Deforestation in Central Africa: estimates at regional, national and landscape levels by advanced processing

of systematically-distributed Landsat extracts. *Remote Sensing of Environment*, **112**, pp. 1969–1981.

ERDAS Inc., 2010, *ATCOR: Atmospheric Correction of Satellite Data, Product Description* (Norcross, GA: ERDAS, Inc.).

ERDAS Inc., 2011, *ATCOR for ERDAS IMAGINE 2011 – User Manual* (Norcross, GA: ERDAS, Inc.).

Frohn, R.C., Hinkel, K.M. and Eisner, W.R., 2005, Satellite remote sensing classification of thaw lakes and drained thaw lake basins on the North Slope of Alaska. *Remote Sensing of Environment*, **97**, pp. 116–126.

Geneletti, D. and Gorte, B.G.H., 2003, A method for object-oriented land cover classification combining Landsat TM data and aerial photographs. *International Journal of Remote Sensing*, **24**, pp. 1273–1286.

Grenier, M., Labrecque, S., Benoit, M. and Allard, M., 2008, Accuracy assessment method for wetland object-based classification. In *Proceedings GEOBIA, 2008 – Pixels, Objects, Intelligence: Geographic Object Based Image Analysis for the 21st Century*, 5–8 August 2008, G.J. Hay, T. Blaschke and D. Marceau (Eds.), Calgary, AB. ISPRS Vol. No. XXXVIII-4/C1. Archives ISSN No.: 1682–1777. pp. 285–289.

Hay, G.J., Marceau, D.J., Bouchard, A. and Dube, P., 2001, A multi-scale framework for landscape analysis: object-specific upscaling. *Landscape Ecology*, **16**, pp. 471–490.

Hui, F., Xu, B., Huang, H., Yu, Q. and Gong, P., 2008, Modeling spatial-temporal change of Poyang Lake using multitemporal Landsat imagery. *International Journal of Remote Sensing*, **29**, pp. 5767–5784.

Jensen, R.J. (Ed.), 2005, *Introductory Digital Image Processing: A Remote Sensing Perspective*, 3rd ed. (Upper Saddle River, NJ: Prentice Hall).

Kuang, W., 2011, Analysis of land use and coverage change (LUCC) and its driving mechanisms in Shaanxi Province: integrating remotely sensed information and the scientific literature. *Resources Science*, **33**, pp. 1621–1629 [in Chinese].

Laflen, J. M., 2000, *Soil Erosion and Dryland Farming* (New York: CRC Press).

Lehner, B. and Doell, P., 2004, Development and validation of a global database of lakes, reservoirs and wetlands. *Journal of Hydrology*, **296**, pp. 1–22.

Li, X., 1995, A new method to improve classification accuracy with shape information. *Journal of Remote Sensing*, **10**, pp. 279–287 [in Chinese].

Liang, S., Fang, H. and Chen, M., 2001, Atmospheric correction of Landsat ETM+ land surface imagery – part I: methods. *IEEE Transactions on Geoscience and Remote Sensing*, **39**, pp. 2490–2498.

Ma, R., Yang, G., Duan, H., Jiang, J., Wang, S., Feng, X., Li, A., Kong, F., Xue, B., Wu, J. and Li, S., 2011, China's lakes at present: number, area and spatial distribution. *Science China Earth Sciences*, **54**, pp. 283–289.

McFeeters, S.K., 1996, The use of the Normalized Difference Water Index (NDWI) in the delineation of open water features. *International Journal of Remote Sensing*, **17**, pp. 1425–1432.

McIver, D.K. and Friedl, M.A., 2002, Using prior probabilities in decision-tree classification of remotely sensed data. *Remote Sensing of Environment*, **81**, pp. 253–261.

Michishita, R., Gong, P. and Xu, B., 2012, Spectral mixture analysis for bi-sensor wetland mapping using Landsat TM and Terra MODIS data. *International Journal of Remote Sensing*, **33**, pp. 3373–3401.

Niu, Z., Gong, P., Cheng, X., Guo, J., Wang, L., Huang, H., Shen, S., Wu, J., Wang, X., Wang, X., Ying, Q., Liang, L., Zhang, L., Wang, L., Yao, Q., Yang, Z., Guo, Z. and Dai, Y., 2009, Geographical characteristics of China's wetlands derived from remotely sensed data. *Science in China Series D: Earth Sciences*, **54**, pp. 723–738 [in Chinese].

Platt, R.V. and Rapoza, L., 2008, An evaluation of an object-oriented paradigm for land use/land cover classification. *The Professional Geographer*, **60**, pp. 87–100.

REN, M.E. and SHI, Y.L., 1986, Sediment discharge of the Yellow River and its effect on the sedimentation of the Bohai and the Yellow Sea. *Continental Shelf Research*, **6**, pp. 785–810.

ROBERTS, N., TAIEB, M., BARKER, P., DAMNATI, B., ICOLE, M. and WILLIAMSON, D., 1993, Timing of the Younger Dryas event in East Africa from lake-level changes. *Nature*, **366**, pp. 146–148.

RUNDQUIST, D.C., LAWSON, M.P., QUEEN, L.P. and CERVENY, R.S., 1987, The relationship between summer-season rainfall events and lake-surface area. *Water Resources Bulletin*, **23**, pp. 493–508.

SCHIEWE, J., TUFTE, L. and EHLERS, E., 2001, Potential and problems of multi-scale segmentation methods in remote sensing. *GIS-Zeitschrift fur Geoinformationssysteme*, **6**, pp. 34–39.

SCHÖOPFER, E., LANG, S. and ALBRECHT, F., 2008, Object-fate analysis: spatial relationships for the assessment of object transition and correpondence. In *Object-Based Image Analysis: Spatial Concepts for Knowledge-Driven Remote Sensing Applications*, T. Blaschke, S. Lang and G.J. Hay (Eds.), pp. 785–801 (Heidelberg: Springer-verlag).

SHENG, Y., SHAH, C.A. and SMITH, L.C., 2008, Automated image registration for hydrologic change detection in the lake-rich Arctic. *IEEE Geoscience and Remote Sensing Letters*, **5**, pp. 414–418.

SIRIKULCHAYANON, P., SUN, W. and OYANA, T.J., 2008, Assessing the impacts of the 2004 tsunami on mangroves using remote sensing and GIS techniques. *International Journal of Remote Sensing*, **29**, pp. 3553–3576.

SIVANPILLAI, R. and MILLER, S.N., 2010, Improvements in mapping water bodies using ASTER data. *Ecological Informatics*, **5**, pp. 73–78.

SOLAIMAN, B., KOFFI, R.K., MOUCHOT, M. and HILLION, A., 1998, An information fusion method for multispectral image classification postprocessing. *IEEE Transactions on Geoscience and Remote Sensing*, **36**, pp. 395–406.

SUN, W., 2004, *Land-Use Classification Using High Resolution Satellite Imagery: A New Information Fusion Method – An Application in Landau, Germany* (Mainz: Johannes Gutenberg University Mainz Press).

SUN, W., HEIDT, V., GONG, P. and XU, G., 2003, Information fusion for rural land-use classification with high resolution satellite imagery. *IEEE Transactions on Geoscience and Remote Sensing*, **41**, pp. 883–890.

TIEDE, D., LANG, S., ALBRECHT, F. and HÖLBLING, D., 2010, Object-based class modeling for cadastre-constrained delineation of geoobjects. *Photogrammetric Engineering and Remote Sensing*, **76**, pp. 193–202.

TOWNSHEND, J.R.G. and JUSTICE, C.O., 1986, Analysis of the dynamics of African vegetation using the normalized difference vegetation index. *International Journal of Remote Sensing*, **7**, pp. 1435–1445.

TRAN, A., GOUTARD, F., CHAMAILLE, L., BAGHDADI, N. and SEEN, D.L., 2010, Remote sensing and avian influenza: a review of image processing methods for extracting key variables affecting avian influenza virus survival in water from Earth observation satellites. *International Journal of Applied Earth Observation and Geoinformation*, **12**, pp. 1–8.

VAN DER WERFF, H.M.A. and VAN DER MEER, F.D., 2008, Shape-based classification of Spectrally identical objects. *ISPRS Journal of Photogrammetry and Remote Sensing*, **36**, pp. 251–258.

VOEROESMARTY, C.J., SHARMA, K.P., FEKETE, B.M., COPELAND, A.H., HOLDEN, J., MARBLE, J. and LOUGH, J.A., 1997, The storage and aging of continental runoff in large reservoir systems of the world. *Ambio*, **26**, pp. 210–219.

WANG, L., SOUSA, W. and GONG, P., 2004, Integration of object-based and pixel-based classification for mangrove mapping with IKONOS imagery. *International Journal of Remote Sensing* **25**, pp. 5655–5668.

WORK, E.A. and GILMER, D.S., 1976, Utilization of satellite data for inventorying prairie ponds and lakes. *Photogrammetric Engineering and Remote Sensing*, **42**, pp. 685–694.

Xu, H., 2006, Modification of normalised difference water index (NDWI) to enhance open water features in remotely sensed imagery. *International Journal of Remote Sensing*, **27**, pp. 3025–3033.

Yu, Q., Gong, P., Clinton, N., Biging, G., Kelly, M. and Shirokauer, D., 2006, Object-based detailed vegetation classification with airborne high spatial resolution remote sensing imagery. *Photogrammetric Engineering & Remote Sensing*, **72**, pp. 799–811.

Zhan, L., 2008, Evaluation of SRTM DEMs' accuracy and investigation on its applicability: a case study in shaanxi province. Master's thesis [in Chinese], Nanjing Normal University, Nanjing.

Zhang, J.X. and Goodchild, M.F., 2002, *Uncertainty in Geographical Information* (New York: Taylor & Francis).